POLITECNICO DI TORINO
Repository ISTITUZIONALE

Progress in the initial design activities for the European DEMO divertor: Subproject "Cassette"

Original
Progress in the initial design activities for the European DEMO divertor: Subproject " Cassette" / You, J., Mazzone, G., Bachmann, Ch., Coccorese, D., Cocilovo, V., De Meis, D., Di Maio, P.A., Dongiovanni, D., Frosi, P., Di Gironimo, G., Garitta, S., Mariano, G., Marzullo, D., Porfiri, M.T., Ramogida, G., Vallone, E., Villari, R., Zucchetti, M.. - In: FUSION ENGINEERING AND DESIGN. - ISSN 0920-3796. - STAMPA. - 124:(2017), pp. 364-370. [10.1016/j.fusengdes.2017.03.018]

Availability:
This version is available at: 11583/2700947 since: 2018-02-22T09:14:54Z

Publisher:
Elsevier Ltd

Published
DOI:10.1016/j.fusengdes.2017.03.018

Terms of use:

This article is made available under terms and conditions as specified in the corresponding bibliographic description in the repository

Publisher copyright

(Article begins on next page)

28 November 2026

Fusion Engineering and Design 124 (2017) 364–370

Contents lists available at ScienceDirect

Fusion Engineering and Design

journal homepage: www.elsevier.com/locate/fusengdes

Progress in the initial design activities for the European DEMO divertor: Subproject "Cassette"

J.H. You[a,*], G. Mazzone[b], Ch. Bachmann[c], D. Coccorese[d], V. Cocilovo[b], D. De Meis[b], P.A. Di Maio[e], D. Dongiovanni[b], P. Frosi[b], G. Di Gironimo[d], S. Garitta[e], G. Mariano[f], D. Marzullo[d], M.T. Porfiri[b], G. Ramogida[b], E. Vallone[e], R. Villari[b], M. Zucchetti[g]

[a] Max Planck Institute for Plasma Physics, Boltzmann Str. 2, 85748 Garching, Germany
[b] ENEA Frascati, Department of Fusion and Technology for Nuclear Safety and Security, via E. Fermi 45, 00044 Frascati, Italy
[c] EUROfusion, PMU PPPT Department, Boltzmann Str. 2, 85748 Garching, Germany
[d] CREATE/University of Naples Federico II, Department of Industrial Engineering,Piazzale Tecchio 80, 80125 Napoli, Italy
[e] University of Palermo, Department of Energy, Viale delle Scienze, 90128 Edificio 6, Palermo, Italy
[f] Sapienza University of Rome Palazzo Baleani, Department of Energetics, Corso Vittorio Emanuele II, 244 – 00186 Rome, Italy
[g] Politecnico di Torino, Department of Energy, Corso Duca degli Abruzzi 24 – 10129 Torino, Italy

HIGHLIGHTS

- A brief overview on the European DEMO divertor cassette design studies is presented.
- Comprehensive computational assessment of multi-physical loads is reported.
- Constraints, impact and implications of predicted loading are explained.
- System performance and rationales of further design optimization are discussed.

ARTICLE INFO

Article history:
Received 13 September 2016
Received in revised form 26 January 2017
Accepted 3 March 2017
Available online 18 March 2017

Keywords:
DEMO
Divertor cassette
Neutronics
Cooling
Thermohydraulics
Electromagnetic loads

ABSTRACT

Since 2014 preconceptual design activities for European DEMO divertor have been conducted as an integrated, interdisciplinary R&D effort in the framework of EUROfusion Consortium. Consisting of two subproject areas, 'Cassette' and 'Target', this divertor project has the objective to deliver a holistic pre-conceptual design concept together with the key technological solutions to materialize the design. In this paper, a brief overview on the recent results from the subproject 'Cassette' is presented. In this subproject, the overall cassette system is engineered based on the load analysis and specification. The preliminary studies covered multi-physical analyses of neutronic, thermal, hydraulic, electromagnetic and structural loads. In this paper, focus is put on the neutronics, thermohydraulics and electromagnetic analysis.

© 2017 The Authors. Published by Elsevier B.V. This is an open access article under the CC BY-NC-ND license (http://creativecommons.org/licenses/by-nc-nd/4.0/).

1. Introduction

Since 2014 preconceptual design activities for developing the divertor of European DEMO reactor have been conducted in the framework of EUROfusion Consortium. The aim of the divertor project (WPDIV) is to deliver a holistic design concept together with the key technologies required for materializing the concept preparing the conceptual design phase. WPDIV is an integrated, interdisciplinary R&D effort where 6 research institutes and 3 university groups are involved.

WPDIV consists of two subproject areas: 'Cassette design and integration' (hereafter 'Cassette') and 'Target development' ('Target'). In the subproject 'Cassette', the overall system of cassette body is engineered whereas in the subproject 'Target' advanced design concepts and key technologies for the plasma-facing components (PFCs) of the targets are developed [1,2].

This design study is based on the baseline CAD configuration model of the European DEMO plant issued in 2015 [3]. The envisaged fusion power is 2037 MW (net electric power: 500 MW). In

* Corresponding author. Jeong-Ha You.
E-mail address: you@ipp.mpg.de (J.H. You).

http://dx.doi.org/10.1016/j.fusengdes.2017.03.018
0920-3796/© 2017 The Authors. Published by Elsevier B.V. This is an open access article under the CC BY-NC-ND license (http://creativecommons.org/licenses/by-nc-nd/4.0/).

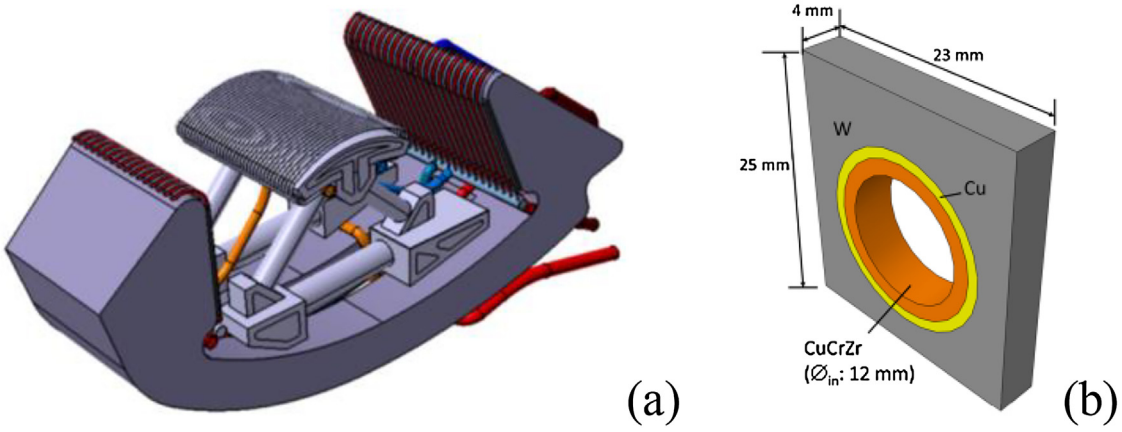


Fig. 1. (a) CAD model of the DEMO divertor cassette and (b) a target PFC mock-up with a schematic of the cross section [1].

this paper, recent results from the WPDIV activities are presented focusing on the subproject 'Cassette' (Fig. 1 [1]).

2. General technical information

In the European DEMO plant design, the divertor consists of 54 separable cassettes. For each set of three cassettes, a lower port is assigned for remote maintenance operation. The DEMO divertor has a reduced size compared to the ITER divertor [4].

In Fig. 2 the sectional geometry of the current cassette model (revised in 2016) is illustrated together with the dimensions. The cassette body has a poloidal extension of 3.02 m, height of 1.97 m and toroidal outer width of 1.04 m. The nominal gap size between two adjacent cassettes will be between 20 and 30 mm. The main body of cassette is made of Eurofer97, reduced activation ferritic martensitic steel. It is divided into chambers separated by stiffening ribs.

The in- and outboard vertical targets are protected by actively cooled PFCs covering the surface. The PFCs and main cassette body are cooled by separate cooling circuits to hold different coolant temperature for each. The primary option for coolant is water for the whole divertor whereas the feasibility of helium cooling is also explored as a low-priority option. The baseline design option for water-cooled PFCs is the ITER-type tungsten monoblock (with a reduced size) with CuCrZr cooling tube [4,5]. In addition, novel PFC design concepts are developed [2].

It is noted that the dome is still regarded as optional and its necessity is currently under extensive assessment.

3. Neutronic analysis

Based on the DEMO plant CAD model of 2015 (with helium-cooled pebble bed blanket), 3D neutronics analysis was carried out using the MCNP5 code and JEFF 3.2 nuclear data [6]. The calculations were normalized to the gross fusion power of 2037 MW which would correspond to a neutron production rate of 7.232×10^{20} n/s.

As the final decision is still open as to whether the dome shall be deployed or not, it was assumed that the entire surface of the cassette body to the plasma was covered with PFCs of the same kind to shield the whole cassette from particles and radiation. It is noted that this is a temporary option to avoid any unrealistic neutronic assessment in the absence of a dome. A consolidated shielding concept is currently devised which shall be employed in case dome is not adopted.

For the neutronics modelling of PFCs, it was assumed that the section of the PFC consisted of 3 homogenized layers where the outermost layers were tungsten and the middle layer was a mixture of tungsten (W: 34 vol.%), water (33 vol.%), CuCrZr (18 vol.%) and copper (Cu: 15 vol.%) representing the actual volume fraction of constituent materials in the PFC.

For the cassette body, water as well as helium was assumed as coolant, for which 3 different cases of materials mixture were considered as follows (volume percent):

1) H_2O-cooled: Eurofer (54%), H_2O (46%)
2) He-cooled: Eurofer (50%), He (50%)
3) He-cooled: Eurofer (30%), He (50%), B_4C (20%)

In the case 3, B_4C cladding was assumed for neutron shielding.

The chemical composition of Eurofer97 steel is given in Table 1. Only the major alloying elements and the impurities of high radiological impact are listed [7].

3.1. Neutron wall loading

The neutron wall load in the divertor exhibits high spatial variability due to the complex geometry. The maximum value amounts to 0.53 MW/m^2 at the upper surface of the cassette which is roughly one half of the maximum neutron wall load at the outboard equatorial first wall (1.33 MW/m^2).

3.2. Nuclear heating

Fig. 3 shows the spatial distributions of nuclear heating power density in Eurofer for the water-cooled (left) and the helium-cooled (right) cases, respectively. It shows that nuclear heating in Eurofer was concentrated near the surface of the cassette and decreased rapidly in the outward radial direction (nota bene: the color code scale is logarithmic). The volumetric heating power density ranged between 0.1 and 6 MW/m^3 for the water-cooled cassette body whereas it varied from 0.2 to 4 MW/m^3 for the helium-cooled case (0.1-3.5 MW/m^3 with B_4C shield).

Table 1
Chemical composition of Eurofer97 steel (wt.%) [7].

Fe	Cr	W	Mn	V	Ta	C	Ni	Mo	Ti	Nb	Al	B	Co
base	9	1.1	0.4	0.2	0.12	0.11	0.01	0.005	0.02	0.005	0.01	0.002	0.01

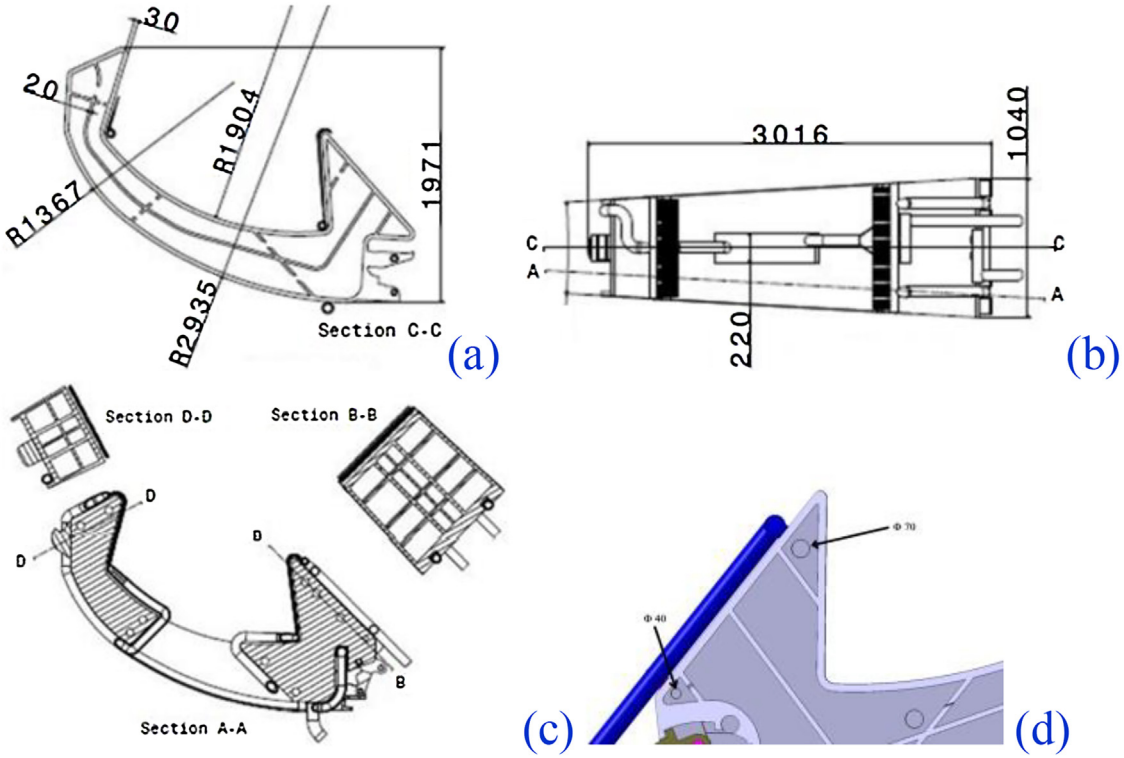


Fig. 2. Sectional geometry and dimensions of the DEMO divertor cassette model as of 2016. (a) toroidal mid-section, (b) radial projection view, (c) toroidal and poloidal cross sections (d) outboard part of a toroidal cut section showing ribs.

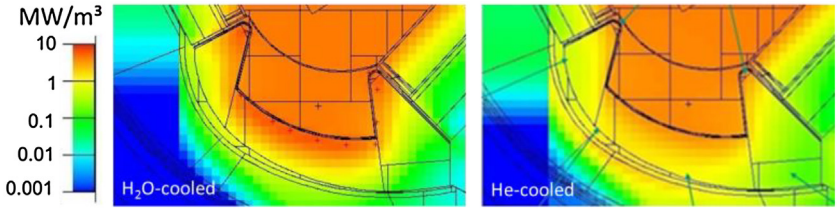


Fig. 3. Spatial distributions of nuclear heating power density in Eurofer in the cassette (left: water-cooled, right: helium-cooled without B_4C shield).

Table 2
Total nuclear heating powers in the major components.

Nuclear heating in 54 cassettes (MW)	H_2O-cooled (H_2O: 46 vol.%)	He-cooled (He: 50 vol.%)	He + B_4C (20%) (He: 50 vol.%)
Inner vertical target	5.4	4.9	3.8
Outer vertical target	8.1	7.0	5.4
PFC skin on cassette body	16.7	14.0	11.3
Cassette body (bulk)	96.1	47.0	55.6
Total	126.3	72.9	76.1

The nuclear heating power in the major components of divertor (in 54 cassettes) is summarized in Table 2. The total nuclear heating power in the entire divertor amounts to 126, 73 and 76 MW for the water-cooled, helium-cooled and helium-cooled with B_4C shield, respectively. The higher heating power in the water-cooled cassette was due to the presence of water where substantial amount of power is deposited contrary to helium. For the underlying vacuum vessel made of SS316L, water-cooling provided more effective shielding (max. 0.7 MW/m^3) compared to the helium-cooled cases (max. 1–1.8 MW/m^3).

In the helium-cooled cases, the presence of the B_4C shield did bring notable shielding effect in the PFCs, but this effect was canceled out by the increased heating power in the cassette body resulting in only minute difference in the total power.

3.3. Lattice damage by irradiation

The maximum values of dpa (displacement per atom) predicted for the major components of the divertor after 2 fpy (full power year) and for the vacuum vessel part locating directly behind the cassette after 6 fpy are summarized in Table 3. The 2 fpy is the envisaged period of continuous service before replacement for maintenance (for vacuum vessel: 6 fpy).

Fig. 4 shows the spatial distributions of irradiation damage rate in the divertor expressed in terms of dpa per fpy (left: water-cooled, right: helium-cooled). The dpa in the copper heat sink was always higher than in the tungsten armor due to the lower energy threshold and higher displacement cross-section of Cu compared to W. The spatial variation of dpa damage amounted to a factor of two for both Cu and W. The higher dpa damage in the PFCs occurred in the

Table 3
Irradiation damage after 2 fpy predicted for the major components of the divertor (in dpa).

Irradiation damage (dpa/2 fpy)	H_2O-cooled (H_2O: 46 vol.%)	He-cooled (He: 50 vol.%)	He + B_4C (20%) (He: 50 vol.%)
Eurofer cassette body	<6	<10	<9
Tungsten armor	1.4–3	1.8–3.2	1.8–3.2
CuCrZr heat sink	6.4–12.8	8.4–14.2	8.4–14.2
SS 316L vacuum vessel (6 fpy)	<1.6	<4.8	<3.9

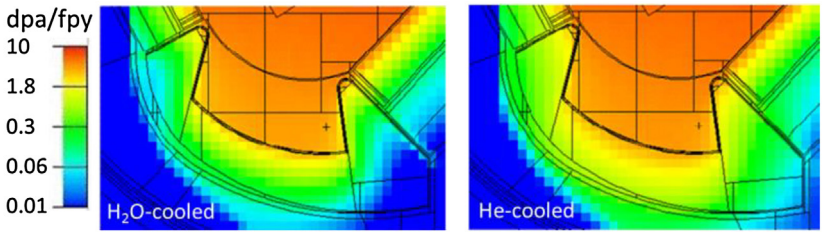


Fig. 4. Spatial distributions of irradiation damage rate (dpa per fpy) in the divertor (left: water-cooled, right: helium-cooled without B_4C shield).

upper region near the blanket while the lower dpa appeared in the lower part of the target around the strike point. Helium-cooling led to slightly higher dpa dose than water-cooling due to moderation of neutron through the steel body and water coolant. The maximum cumulated dose in the W armor after 2 fpy (specified PFC lifetime) reached 3 dpa for water- and 3.2 dpa for helium-cooling. In the CuCrZr tube, the maximum dose was 12.8 dpa for water- and 14.2 dpa for helium-cooling. According to the previous irradiation test data, CuCrZr exhibits saturation of tensile behavior in the dose range of 0.5-2.5 dpa [8] or 1–10 dpa [9] at 150–300 °C. Thus, the peak dpa values (13–14 dpa) may probably be acceptable.

The maximum accumulated damage in the steel cassette body was 6 dpa (after 2 fpy) for water-cooling whereas it reached 10 dpa for helium-cooling (9 dpa with B_4C shield). If the water coolant temperature is kept above 180 °C in the cassette body, then 6 dpa would be acceptable for Eurofer steel as the shift of the fracture toughness transition temperature by irradiation up to 6 dpa still does not bring the steel into fully embrittled state [10]. For the helium-cooled case, the inlet coolant temperature will have to be higher than 210 °C to avoid full embrittlement of the steel body at 9–10 dpa. The dpa profiles exhibited rapid decline in the radial direction. In the outer bottom region the dose decreased down to 0.02 dpa in the water-cooled cassette. In the helium-cooled case, the dose in the same region was one order of magnitude higher due to reduced shielding capability.

The cumulative damage in the vacuum vessel (SS 316L) after 6 fpy was 1.8, 4.8 and 3.9 dpa for the water- and helium-cooled cases with and without B_4C shield, respectively. It is noted that the allowed dpa limit specified for the austenitic stainless steel is 2.75 dpa at which the fracture toughness is reduced by no more than 30% [11]. Water-cooling ensures sufficient neutron shielding for the vacuum vessel while it does not seem to be the case for the helium-cooling cases.

3.4. Helium transmutation

Formation of helium bubbles by transmutation causes severe embrittlement and swelling affecting reweldability required for remote maintenance. The maximum helium production in the steel cassette body reached 100 appm after 2 fpy. The assumed boron content in Eurofer97 was 0.002 wt.% (Table 1) which is the maximum allowable impurity concentration limit for boron defined in the F4E specification [7]. The helium concentration limit below which rewelding using electron beam is supposed to be possible is 1–3 appm [11] being two orders of magnitude lower than the predicted maximum value on the plasma-facing surface. For ensuring reliable rewelding of cooling pipes, the cutting zone has to be located in the outermost outboard region sufficiently shielded by the blankets and cassette itself.

3.5. Forthcoming analyses

The next neutronics analysis campaign will include the effect of the dome, realistic distribution of materials in a refined CAD model and revised divertor cassette layout (e.g. port plug in the lower domain for shielding the vacuum vessel).

4. Cooling scheme and thermohydraulic analysis

4.1. Operation temperature range for the water-cooled cassette

The baseline cooling concept is based on water-cooling while helium-cooling is considered as advanced design option. In this paper, discussion is focused on the water-cooling case.

It is one of the basic design requirements that the structural material of the cassette body (i.e. Eurofer steel) be operated in such a way that uncontrolled fast fracture is avoided. In this design study, fracture toughness transition temperature (FTTT) was employed as measure of critical temperature band across which the material state in the crack-tip region rapidly changes from ductile to brittle. As FTTT is measured using precracked specimens, it is regarded more conservative compared to DBTT (ductile-to-brittle transition temperature) by impact tests. The lower operation temperature limit of irradiated Eurofer can be defined according to the FTTT data at 6 dpa as follows [12]: >180 °C (with He production) or >120 °C (no He production). The upper service temperature limit of Eurofer97 is known to be around 550 °C, above which the steel rapidly loses strength. The thermohydraulic design for cooling the steel cassette body should respect these temperature constraints.

4.2. Water-cooling of cassette body

The interior of the cassette body is divided into many chambers separated by ribs (20 mm thick) each with a hole (diameter: 40–70 mm) through which the pressurized coolant is guided to flow. A schematic view of the cassette interior is illustrated in Fig. 5(a). The outlet and inlet coolant feeding pipes connected to the outboard edge face are shown. The layouts of the feeding pipes, ribs and holes were optimized on the basis of iterative CFD simulations. The rectangular cross section of the cassette body consisted of lattice-like chambers. The middle poloidal rib separates the inlet

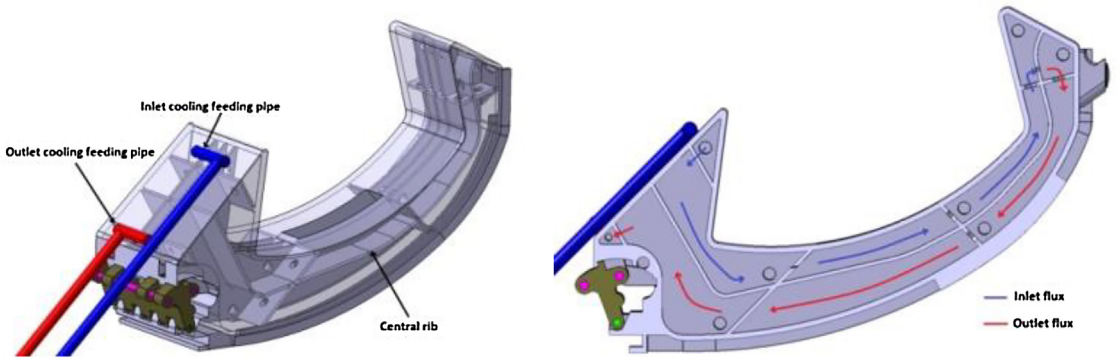


Fig. 5. A schematic view of the cassette interior with the inlet and outlet coolant feeding pipes on the outboard boundary face (left) and a poloidal cut section of the cassette (right) where the direction of coolant flow is schematically illustrated.

Table 4
Input parameters considered for CFD analysis of the water-cooled cassette body and the predicted results of thermo-hydraulic performance.

H_2O-cooled cassette	Pipe design 1	Pipe design 2
Coolant inlet temp. (°C)	150	180
Coolant inlet pressure (MPa)	3.5	3.5
Mass flow rate (kg/s)	308	861
Coolant outlet temp. (°C)	220	210
Pressure drop (MPa)	0.01	0.1
Pumping power (kW)	4	93
Coolant max. temp. (°C)	242 (at the wall)	214 (at the wall)
Cassette body temp. (°C)	<330	<330

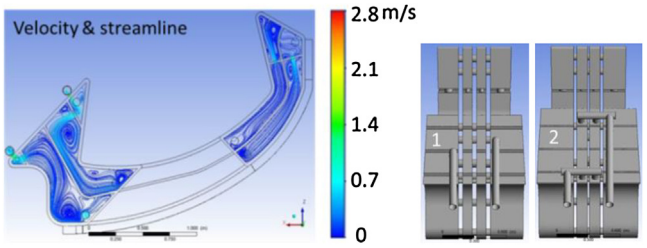


Fig. 6. Streamlines and speed of the water coolant flowing in the divertor cassette (left). Two different design concepts of the cooling pipe connections to the cassette body (right).

and outlet coolant streams (see Fig. 5(b)). The outer shell plate is 30 mm thick.

To assess the cooling performance of the water-cooled cassette body, full 3D thermohydraulic analysis was carried out based on finite volume method using commercial computational fluid dynamics (CFD) code, ANSYS-CFX (v16). The input coolant parameters and the results of 3D CFD analysis are summarized in Table 4. Details of the CFD simulation are found elsewhere [13,14].

In Fig. 6, the streamlines of water coolant are plotted together with the speed distribution in color code. In general, the water flow exhibits a reasonable streamline pattern, but two large vortices formed in the outboard region need to be reduced by further optimization of the rib structure.

It is found that the water-cooling case exhibits a reasonable thermal and hydraulic performance. Particularly, water-cooling is beneficial in terms of the low pumping power (4 kW in total) and high heat capacity. The maximum temperature developing in the steel body was far below the maximum allowable service temperature limit (550 °C). The water coolant bulk was heated up to 220 °C in the outlet region. The maximum temperature in the coolant reached locally up to 242 °C in the thin boundary layer near the inner surface which was close to the vaporization temperature at the given pressure. For increasing the margin to film boiling water, mass flow rate needs to be increased.

Table 5
Thermohydraulic performance of the water-cooled target PFC predicted for three different cooling options.

per cassette	Option 1	Option 2	Option 3
Mass flow rate (kg/s)	60	110	60
Temperature rise (°C)	9	5	9
Pressure drop (MPa)	1.4	1.5	1.8
Min. velocity (m/s)	17	15	15
Min. CHF margin	1.6	1.6	1.4

4.3. Water-cooling of target PFCs

The thermohydraulic performance of the water-cooled divertor target PFC was assessed by means of 3D CFD simulations. The target PFCs are exposed to high heat flux loads generated by radiation (53 MW), plasma bombardment (39 MW) and nuclear heating (14 MW). This means that 54 in- and outboard target plates have to exhaust the deposited thermal power of 106 MW in total. At the plasma strike point the maximum power density was assumed to reach about 20 MW/m^2 during slow transients (loss of plasma detachment) in 2–3 s. During a quasi-stationary operation (pulse duration: 2 h) the heat flux density profile was assumed to range from 1 to 10 MW/m^2 [15]. The power exhaust capability has to be assured in terms of global energy balance as well as local margin to critical heat flux (CHF) at the tube wall. To this end, a highly efficient cooling scheme and technologies are demanded.

In WPDIV, three different options of cooling circuit have been devised and estimated (Fig. 7). Following coolant parameters were assumed for the PFCs as CFD boundary conditions [2]:

- Peak heat flux density at strike point: 20 MW/m^2
- Heat flux peaking factor at the tube wall: 2
- Coolant temperature: 150 °C (PFC inlet)
- Coolant pressure: 5 MPa (PFC inlet)
- Mass flow rate per pipe in PFC: 1.67 kg/s

The results of the comparative CFD analysis are summarized in Table 5. All three options allow sufficient margin to the CHF at the strike point for the applied surface heat flux. It is noted that the recommended margin to CHF is 1.4 at least. The rise of coolant temperature looks also moderate for all three cases.

On the other hand, pressure drop is quite significant, especially for option 3. Another concern is the high coolant speed locally peaking up to 20 m/s so that corrosion-erosion of pipe wall is fostered. The outcome of this CFD analysis implies that the peak coolant speed needs to be reduced by decreasing the inlet water tempera-

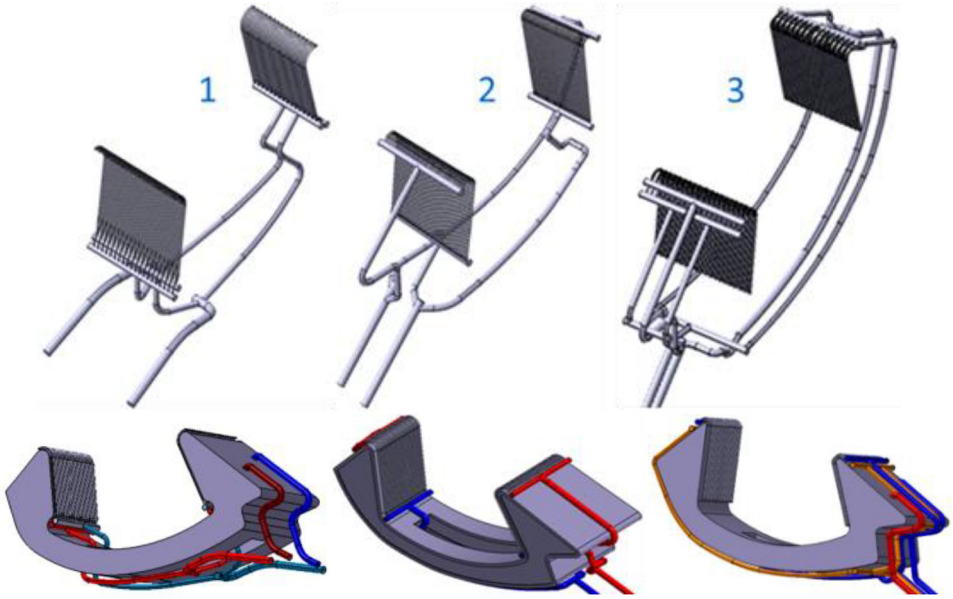


Fig. 7. Three different cooling scheme options considered for the thermohydraulic design of the divertor target plate.

ture and/or increasing the tube radius. A follow-up investigation is ongoing targeting the coolant speed of about 10 m/s, pressure drop below 1.4 MPa and CHF margin higher than 1.4. Here, the operation temperature range recommended for the irradiated CuCrZr heat sink tube (structural material) by the structural design code ITER SDC-IC imposes constraint on the applicable coolant temperature [16,17]. For relaxing such constraint, advanced design rules based on non-ductile fracture mechanics can be employed so that the use of low-temperature operation of divertor PFCs is justified.

5. Electromagnetic force analysis

Global plasma instabilities such as plasma disruptions and vertical displacement events (VDEs) induce or generate huge transient electric currents in the conductive steel cassette body. Disruptions induce eddy currents whereas VDEs generate halo currents. The interaction of the currents with the magnetic field induces Lorentz force ($\vec{F}=\vec{J}\times\vec{B}$) as impact load. Particularly, the force induced by a VDE can impose a critical impact on the divertor due to high current density. In WPDIV, finite element method (FEM)-based 3D electromagnetic analysis was carried out to assess such impact loads assuming various parametric combinations. In this paper, only the result for the most critical case is presented (product of halo fraction and toroidal peaking factor: 1, halo current partition ratio between the main body and other parts: 1). The duration time of linear current quench was assumed to be 50 ms [18] (For DEMO, it was revised to 70 ms [19]). It was assumed that plasma disruption began 10 s after the initiation of fast discharge (characteristic time: 27 s). Contact resistance was neglected. The radial decay of toroidal magnetic field ranged from 8.3 T to 5.6 T (nominal B_T: 5.6 T).

5.1. Halo current

Fig. 8 illustrates the electric potential field generated by a VDE in color code (left) together with arrows indicating the current path and direction (right). The electric potential built up along the poloidal direction from the inboard top toward the outboard end forming the halo current path. The maximum halo current density reached 2.2 MA/m^2. Concentration of current density occurred locally at the shell edges and corners.

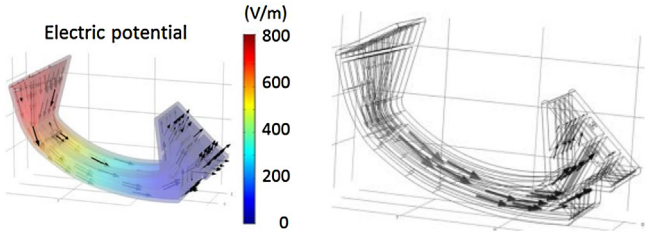


Fig. 8. Electric potential field generated by a VDE (left) and halo current path indicated with arrows (right).

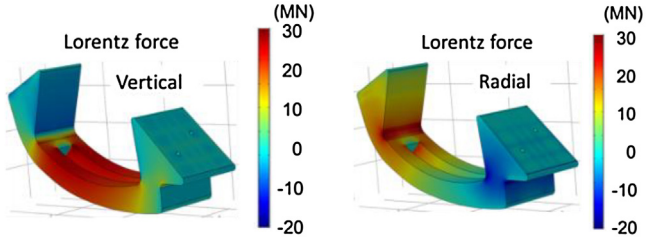


Fig. 9. Induced Lorentz forces in the divertor cassette shell plate (left: vertical, right: radial component).

5.2. Lorentz forces and stresses

The induced Lorentz forces in the shell plate are plotted in Fig. 9 (left: vertical, right: radial component). Strong upward vertical force appeared in the middle part of the cassette body (30 MN) and downward vertical force in the inboard and outboard wings (10 MN). The upward vertical force causes (elastic) deformation of the middle part where the displacement reaches up to 1.4 mm upwards.

Fig. 10 shows the induced stress fields (von Mises stress) in the outer shell plate (left) and in the internal ribs (right). The stress state in the entire cassette structure remained in the elastic regime even in the most severe loading case considered in this analysis. This result indicates that the cassette body is robust enough to withstand the transient electromagnetic impact loads caused by plasma VDEs.

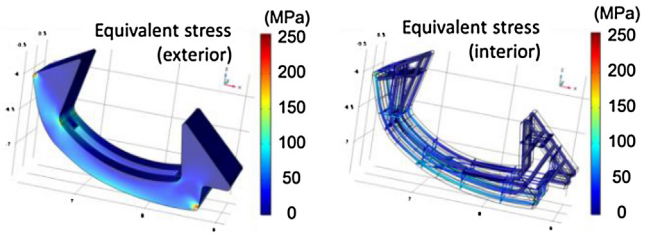


Fig. 10. Induced stress field (von Mises equivalent stress) in the shell plate (left) and in the internal ribs (right).

6. Other activities

In subproject "Cassette", other activities are being performed as well. Examples are: FEM-based structural analysis and code-based design study, optimization of CAD models, development of cassette fixation scheme, experimental verification of CFD, and functional analysis, etc. (will be reported elsewhere.)

7. Conclusions

The initial design exploration study in the preconceptual design phase to develop European DEMO divertor has been recently concluded. In the subproject 'Cassette design and integration', following results are the major achievements:

1 CAD: complete 3D configuration model was created.
2 Neutronics: the radiological impact was analyzed for the case dome is not deployed. Armoring of cassette surface with the PFCs similar to the target necessitated improved shielding.
3 Thermohydraulics: for both target PFCs and cassette body, the current design of water-cooling circuits seemed adequate.
4 Electromagnetic analysis: the current cassette model seemed to be robust enough to accommodate VDE impact loads.

Acknowledgment

"This work has been carried out within the framework of the EUROfusion Consortium and has received funding from the Euratom research and training program 2014–2018 under grant agreement No 633053. The views expressed herein do not necessarily reflect those of the European Commission."

References

[1] J.H. You, et al., Fusion Eng. Des. 109–111 (2016) 1598–1603.
[2] J.H. You, et al., Nucl. Mater. Enerrg 9 (2016) 171–176.
[3] C. Bachmann, et al., Fusion Eng. Des. 112 (2016) 527–534.
[4] R.A. Pitts, et al., J. Nucl. Mater. 415 (2011) S957–S964.
[5] F. Crescenzi, et al., ITER-like divertor target for DEMO: design study and fabrication test, Fusion Eng. Des. (2017) (submitted).
[6] www.oecd-nea.org/dbforms/data/eva/evatapes/jeff_32.
[7] Technical specifications EUROFER material database, F4E-2008-GRT-010 (PNS-MD).
[8] W. Timmis, Material Assessment Report on the Use of Copper Alloys in DEMO EFDA Report WP12-MAT02-M03, 2013.
[9] P. Fenici, et al., J. Nucl. Mater. 212–215 (1994) 399–403.
[10] E. Gaganidze, J. Aktaa, Fus. Eng. Des. 88 (2013) 118–128.
[11] V. Barabash, et al., J. Nucl. Mater. 367–370 (2007) 21–32.
[12] G. Mazzone, et al., Fusion Eng. Des. (2017), http://dx.doi.org/10.1016/j.fusengdes.2017.02.013.
[13] P.A. Di Maio, et al., Fusion Eng. Des. (2017), http://dx.doi.org/10.1016/j.fusengdes.2017.02.012.
[14] P.A. Di Maio, et al., Fusion Eng. Des. (2017), http://dx.doi.org/10.1016/j.fusengdes.2017.02.025.
[15] R.P. Wenninger, Nucl. Fusion 54 (2014) 114003.
[16] J.H. You, Nucl. Mater. Energy 5 (2015) 7–18.
[17] J.H. You, Nucl. Fusion 55 (2015) 113026.
[18] T.C. Hender, et al., Ch.3. MHD stability, operational limits and disruptions, Nucl. Fusion 47 (2007) S128–202.
[19] C. Bachmann, DEMO Plant Structural Load Specification, EFDA_D_2MY7H3, 2017.